A Second Site Rescue Mutation Partially Restores Functional Expression to the Serotonin Transporter Mutant V382P†

Irache Visiers,‡,§ Harel Weinstein,‡ Gary Rudnick,|| and Megan M. Stephan*,||

Department of Pharmacology, Yale University School of Medicine, 333 Cedar Street, New Haven, Connecticut 06510, and Department of Physiology and Biophysics, Mount Sinai School of Medicine, New York, New York 10029-6574

Received December 11, 2002; Revised Manuscript Received April 9, 2003

ABSTRACT: Transmembrane span 7 (TM7) of the serotonin transporter (SERT) was previously subjected to random mutagenesis, and the mutation V382P was found to abolish transport activity. Val-382 lies next to a threonine residue in the native sequence, creating a TP motif in this mutant. On the basis of molecular modeling studies, which have shown that the presence of a TP motif produces a very large kink in an α-helix, it was hypothesized that this motif could be the source of V382P's deleterious effects. We tested this hypothesis by producing second site mutations in the V382P construct that removed the TP motif: T381A-V382P and T381V-V382P. These mutants were tested for the recovery of serotonin transport and binding activities and for expression at the cell surface. The TM7 α-helix was modeled computationally, using Biased Monte Carlo simulations to quantify the conformational preferences of the wild type and mutant helices. The double mutation T381A-V382P, which was predicted by modeling to produce a smaller perturbing bend in TM7, was indeed found to allow partial rescue of transport activity. The double mutation T381V-V382P, on the other hand, did not rescue transport activity. Computational analysis of this mutant predicted a markedly different conformational preference from either the V382P or the T381A-V382P mutants. These studies show that changes in the structure of TM7 exert a strong influence on SERT's ability to achieve a mature, properly folded, cell surface conformation.

The serotonin transporter (SERT)[1] is responsible for the removal of 5-hydroxytryptamine (5HT, serotonin) from the synaptic cleft following neurotransmission. SERT belongs to the neurotransmitter/sodium symporter (NSS) family, a large family of highly homologous neurotransmitter and amino acid transporters including transporters specific for serotonin, dopamine, norepinephrine, GABA, glycine, proline, creatine, taurine, and betaine (*1*). These transporters are located in the plasma membrane where they mediate the translocation of their substrates from the synapse to the interior of the cell. This process is energetically coupled to the cotransport of Na^+, Cl^-, and K^+ ions across the membrane (for reviews, see refs *2*−*4*). Hydrophobicity analysis of a sequence alignment of these proteins predicts that each contains 12 transmembrane segments (TMs) connected by intracellular and extracellular loops. Experimental efforts have elaborated elements of SERT topology, including evidence that both the N and the C termini are intracellular and that predicted intracellular loop 3 and all of the extracellular loops are positioned roughly as predicted by hydropathy analysis (*5*−*7*).

The detailed molecular organization of SERT is still poorly understood since a high-resolution structure has yet to be elucidated. Various experimental approaches have been used to test the basic structural prediction regarding the 12 TMs and to correlate functional information with the molecular mechanisms by which the Na^+ and Cl^- gradients are coupled to the inward movement of serotonin. The high homology among the proteins of this family makes it reasonable to assume that they share a common scaffold, as well as a common basic mechanism of action, so that structural and functional inferences obtained from one transporter can be extrapolated to the other proteins in the same family (*8*). This approach has been used extensively and with great success for the determination of the structure and function of G protein-coupled receptors (see ref *9* for a review).

Transmembrane span 7 (TM7) of SERT has been subjected to extensive site-directed mutagenesis. The pattern of sensitivity to mutation in this stretch of amino acid residues has led to the conclusion that TM7 forms an α-helix, one side of which plays a critical structural and/or functional role in the transporter (*10*). In the dopamine transporter (DAT), native and engineered Zn^{2+} binding sites have been used to probe both secondary and tertiary structure relations in this region. These studies also show that TM7 is likely to be helical and that it lies in close contact with TM8 (*11*−*13*). Other investigators have also concluded that TM7 plays a functionally important role in DAT (*14*−*17*).

The different responses of positions in TM7 to mutation suggest that this TM has special conformational properties that can determine the correct folding and/or functionality

† This work was supported by grants from the National Institute on Drug Abuse, DA12586 to M.M.S. and DA012408 to G.R. and H.W.

* To whom correspondence is to be addressed. Telephone: (203) 737-1601. Fax: (203) 785-7670. E-mail: megan.stephan@yale.edu.

‡ Mount Sinai School of Medicine.

§ Current address: Millennium Pharmaceuticals, Inc., 75 Sidney St., Cambridge, MA 02139.

|| Yale University School of Medicine.

[1] Abbreviations: 5HT, serotonin; SERT, serotonin transporter; TM, transmembrane span; WT, wild type.

10.1021/bi0273415 CCC: $25.00
Published on Web 05/14/2003

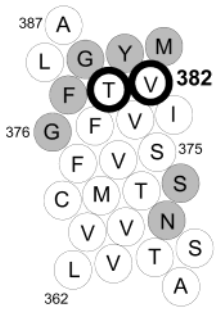

FIGURE 1: Helical net representation of TM7 from SERT. Bold circles indicate residues Thr-381 and Val-382. Shaded circles are functionally important residues identified in ref *10*.

of the protein. Among the mutations in this span, the replacement of Val-382 by proline was shown to abolish transport activity. However, substitutions by proline at other positions of the helix, for example, in the adjacent 381 position, were well-tolerated (Figure 1) (*10*). Prolines are known to disrupt the structure of α-helices by introducing a kink between the segments preceding and following the proline residue (see refs *18* and *19* and references therein). The kink induced by a proline in an α-helix can be modulated by the residues surrounding the proline, and as shown in earlier studies, this modulation can be reflected in the functional properties of the constructs (*20*). In particular, the presence of a threonine in the position preceding the proline creates a special motif, called a TP motif (*20*). In this motif, the threonine residue can form a hydrogen bond with the carbonyl four residues upstream that is freed by the lack of hydrogen bonding to the cyclized nitrogen of the proline. This bond stabilizes the larger bend of the proline kink. Interestingly, SERT has a threonine at position 381, which in combination with the proline introduced by random site-directed mutagenesis at position 382 would yield a TP motif that is expected to produce an especially large kink (*20*−*22*). The structural implication of the observed loss of function after the introduction of a proline at position 382 is, therefore, that distortion of the TM7 helix is the detrimental perturbation.

To test the hypothesis that an especially large kink induced in the helix by the TP motif in mutant V382P could be responsible for the loss of transport activity, we investigated the effect of the residue preceding Pro-382, both experimentally and using computational simulations. For the latter, we used Biased Monte Carlo simulations to quantify the conformational preferences of TM7 in wild-type SERT (WT) as compared to three mutants: the original V382P (TP) mutant and two double mutants in which Thr-381 was substituted with alanine or valine. The computational studies provide evidence that the kink induced by the proline at position 382 can be modulated by substitutions at the 381 position. These results were used to interpret the experimental results obtained for the mutants. The double mutation T381A-V382P (AP), which eliminates the TP motif and is predicted to have a smaller perturbing bend in TM7, was indeed found to allow partial rescue of transport activity. The double mutation T381V-V382P, on the other hand, which also eliminates the TP motif, did not rescue any transport activity. However, computational analysis shows that this mutant is predicted to have a different conformational preference from either the TP or the AP mutants, and this conformation also appears to prevent SERT from reaching a mature, properly folded, cell surface conformation.

EXPERIMENTAL PROCEDURES

I. Computational Simulations of Wild Type and Mutant TM7 Structures. Construction of the TM7 Helix. The sequence used for the conformational study comprises residues 362−390 of the rat brain serotonin transporter, and the helix was built using the CHARMM package (*23*). Four different constructs were built corresponding to TM7 of each of the four transporter proteins tested experimentally: WT and mutants V382P (TP), T381A-V382P (AP), and T381V-V382P (VP). The WT construct was built as an ideal α-helix, whereas the starting TM7 for each of the mutant constructs was built with a standard proline kink as described in (*24*).

Exploration of the Conformational Space. The structural characteristics of the kink introduced in the helix by proline in the different mutant constructs were investigated by exploration of their conformational space using Biased Monte Carlo (BMC) simulations and computation of the parameters that define the proline kink described earlier (*19*).

The BMC method used in this study is the Conformational Memories (CM) method (*25*, *26*), a two-stage method consisting of an exploratory phase and a biased sampling phase. In the exploratory phase, several Monte Carlo simulated annealing (MC/SA) runs were performed to a final temperature of 310 K. For the four peptides studied here, the starting temperature was sufficiently high (3000 K) to guarantee randomization of the starting structures. The cooling schedule was $T_{n+1} = 0.9T_n$, and the interval of temperatures was divided into 18 steps; 10^4 trial moves per temperature were generated. Trial conformations were obtained by randomly picking two rotatable dihedral bonds among all the dihedral angles of residues at positions 378−382 and assigning random values between ±180° (peptide bonds were considered fixed at 180° throughout the simulation). There are 78 rotatable bonds in this sequence fragment, so random trial moves on each one of those 78 bonds generated one block of information (78 in total). Each rotatable bond block was divided into 18 temperature blocks, and the dihedral space was partitioned into 36 10° intervals with normalized populations. After each trial move, acceptance of a trial conformation followed the standard Metropolis algorithm with a Boltzmann distribution. The spreadsheet containing these data represented the dihedral distribution of a given torsional angle in the mean field of all other rotatable bonds. The MC/SA phase of the BMC simulation included 60 runs, each one comprising a complete set of trial moves as described above.

The information about the dihedral distribution obtained in the MC/SA phase was used in the second phase of the simulation, in which the Monte Carlo sampling explores only the populated regions of the conformational space weighted by the probability distribution generated in the first phase (*26*). In this second phase, the ensembles of the populated regions of the conformational structures at 310 K were obtained from a second simulated annealing starting from $T = 850.1$ K and cooling to 310 K in 160 000 steps, with sampling performed only from the populated regions of the conformational memories. After several runs were performed, a probability distribution of each torsional angle in the mean

field of all other rotatable bonds was obtained at the lower temperature. The conformational properties of the various constructs were analyzed with respect to the proline-related perturbations as described below.

Characterization of the Conformational Space. Once the conformational space had been thoroughly explored, results obtained for the different constructs were analyzed by comparison of the distortion that proline produces in the helix in the distinct mutant constructs.

A detailed geometric definition of the kink induced by proline in the helix, and the software for numerical evaluation of the parameters describing it (Prokink), have been reported in detail elsewhere (*19*). Briefly, we quantify the conformational perturbation from the helix coordinates, in terms of two proline-related parameters: the bend angle (θ_b) and the wobble angle (θ_w). The definition of the proline kink involves two segments of the helix: from the N-terminus to the proline residue and from the proline residue to the C-terminus. The bend angle is the angle between the two segments when the helix is kinked along its axis. The wobble angle is the angle of rotation of the helix segment following the proline around a screw axis, which is the axis of the helix preceding the proline (*18*, *19*). This angle defines the orientation of the bend in space (for a more detailed explanation of these parameters see refs *18* and *19*). To characterize the structural differences among the various constructs, we calculated the energy weighted average values of the bend and wobble angles (see above) generated in the Monte Carlo runs from

$$\langle\theta\rangle = Z^{-1}\sum_{i=1}^{N}\theta_i \exp(-E_i/kT) \quad (1)$$

where E_i is the energy of the system in the helix conformation i in the ensemble, and N denotes the number of conformations necessary for convergence; Z is the partition function of the system in the ensemble, k is the Boltzmann constant, and the temperature was fixed at $T = 310$ K. This weighted average of the angle over the conformational space $\langle\theta\rangle$ considers the probability of each structure adopting the angle value by taking into account its energy E_i.

Energy Weighted Parsing of the Conformational Space. To obtain a quantitative analysis of the distribution of the constructs in the conformational space, we bin the range of values of the angle θ that characterizes the bend and wobble angles and calculate the population of each bin. The best intervals were determined by manually parsing the spectrum of angle values in different size bins and choosing the interval size that yielded the best separation of the population of each one of the bins. The population of each bin is expressed as an energy weighted probability $P_i(\theta)$ of finding a structure in each bin, which is given by

$$P_i(\theta) = Z^{-1}\sum_{i=1}^{N_i} \exp(-E_i/kT) \quad (2)$$

where N_i is the number of structures with θ in bin i, E_i is the energy of the system in the helix conformation i in the ensemble, Z is the partition function of the system in the ensemble, k is the Boltzmann constant, and the temperature was taken as $T = 310$ K.

II. Construction and Analysis of TM7 Mutants. *Materials.* Plasmid DNA was prepared using Qiagen midiprep kits (Qiagen, Inc., Valencia, CA). Restriction fragments were purified from agarose gels using the Geneclean kit (Bio-101, Inc., Vista, CA). All other reagents were obtained from Sigma Chemical Co. (St. Louis, MO) unless otherwise indicated.

Construction of New Mutants. All SERT mutants in this study were produced using the PCR-based megaprimer method. This method, which has been described in detail elsewhere (*10*, *27*−*29*), uses three primers: one mutagenic primer and two nonmutagenic primers that lie outside the region to be mutated and are used solely for amplification. In the first round of PCR, the mutagenic primer and one outside primer were used to amplify a partial fragment of the region where the mutation was to be added. This mutagenized fragment was purified and used as a megaprimer, together with the second outside primer, in a second round of PCR to amplify the entire region to be subcloned. The resulting PCR fragment was then cut with appropriate restriction enzymes and subcloned back into the wild-type plasmid.

Plasmid pRSTag carries a cDNA encoding the rat brain serotonin transporter, with the addition of sequences encoding a *c-myc* epitope tag at the N-terminus and a FLAG epitope tag at the C-terminus (*30*). We had previously used site-directed mutagenesis to add a silent mutation at base pair 1273, creating a new, unique MfeI restriction site (plasmid pRSTagM). SERT mutant V382P was created in this background by using a random mutagenesis variation of the megaprimer method (*10*). In the present study, the megaprimer method was used to add mutations T381A and T381V to the V382P mutant and to wild-type SERT. After subcloning, each mutant plasmid was screened for the presence or absence of silent restriction sites included in the mutagenic primers, indicating the presence or absence of the desired mutations. A large plasmid preparation of each positive colony was then made and retested for the presence or absence of the screening sites. Plasmid preparations were also tested with the diagnostic enzymes PvuII and PstI to detect any major rearrangements, insertions, or deletions in the SERT cDNA. All mutants were also sequenced in both directions between the subcloning sites to confirm the presence of the desired mutations and to ensure that no extraneous mutations had been incorporated during the PCR reactions.

Expression of Mutant SERTs. The expression system used has been described in detail elsewhere (*31*−*33*). Briefly, the plasmid pRSTagM contains a promoter for T7 RNA polymerase upstream from the rat brain SERT cDNA. This promoter was used to express wild type and mutant SERTs in the vaccinia/T7 polymerase/HeLa cell system. HeLa cells were plated in 48 well plates at 50% confluency and allowed to grow overnight in DMEM supplemented with 10% fetal bovine serum, 100 units/mL penicillin G, and 100 μg/mL streptomycin sulfate (GIBCO-BRL, Gaithersburg, MD). The next day they were infected with a vaccinia virus strain, VTF7−3 (*32*), which makes T7 RNA polymerase (virus was added to the cells in 50 μL/well DMEM without serum). After a 15 min incubation with the virus at 37 °C, the cells were transiently transfected with wild type and mutant plasmids (400 ng of plasmid DNA and 1.2 μL of Lipofectin

(GIBCO-BRL) per well in 100 μL of DMEM without serum). Wild-type SERT, no plasmid (mock-transfected) controls, and mutants were each transfected in duplicate wells.

Transport Assays. [^{3}H]-Serotonin transport assays were carried out the next day between 19 and 24 h post-infection. For the standard assay, cells were washed twice with 200 μL of phosphate-buffered saline (PBS; 137 mM NaCl, 2.7 mM KCl, 4.3 mM Na_2HPO_4, and 1.4 mM KH_2PO_4, pH 7.3) containing 0.1 mM $CaCl_2$ and 1 mM $MgCl_2$ (PBSCM). Transport was measured by incubating the cells with 14.6 nM [1,2-^{3}H(N)]-serotonin (Dupont-New England Nuclear, Inc., Boston, MA; #NET-498) in 80 μL of PBSCM. Transport was measured at 10, 20, 30, 40, 50, and 60 min by washing the appropriate wells three times in 20 s with 200 μL of ice-cold PBS. The cells were lysed in 300 μL of 1% SDS, transferred to scintillation vials, and counted in 3 mL Optifluor (Packard Instrument Co., Meriden, CT).

Binding Assays. Binding of the cocaine analogue 2β-carbomethoxy-3β-(4-[^{125}I]-iodophenyl)-tropane (β-CIT; Dupont-New England Nuclear #NEX272) was measured in crude membrane preparations. HeLa cells were grown, infected, and transfected as described above except in 75 cm^2 tissue culture flasks, with appropriate scaling up of all reagents. After overnight transfection/infection, the cells were rinsed twice with 12 mL of room-temperature lithium-phosphate buffer (150 mM LiCl, 1.4 mM KH_2PO_4, 4.3 mM K_2HPO_4, 0.1 mM $CaCl_2$, and 1 mM $MgCl_2$, pH 7.5) per flask. They were harvested by scraping each flask into 4 mL of ice-cold Li-HEPES buffer (10 mM HEPES free acid brought to pH 8.0 with LiOH) containing 0.5% of a protease inhibitor cocktail (Sigma Protease Inhibitor Cocktail; #P8340). The cells were lysed by two cycles of freeze−thawing and sonication: freeze −80 °C, 15 min; thaw 37 °C, 10 min; and sonicate in bath filled with ice water, 3 min. The resulting crude mixture of membranes was collected by centrifugation at 15 000*g* for 20 min at 4 °C. After removal of the supernatant, the membrane pellet was resuspended in 1 mL of ice-cold Li-HEPES buffer with protease inhibitors per flask and frozen at −80 °C in 125 μL aliquots.

For binding assays, aliquots of membranes from cells expressing mutant and wild-type transporters were thawed on ice and diluted 7× with ice-cold binding buffer (10 mM Na-HEPES (pH 8.0), 300 mM NaCl, 1 mM $MgCl_2$, 0.1 mM $CaCl_2$). Binding was measured in 96-well filtration plates containing glass fiber filters (Multiscreen-FB, Millipore Corp., Bedford, MA). The plates were prepared the night before by the addition of 200 μL of 0.1% polyethyleneimine (PEI) to each well and incubation at 4 °C overnight. The PEI was rinsed away with 3 × 200 μL room-temperature binding buffer. Each well then received 30 μL of the appropriate concentration of [^{125}I]-β-CIT, mixed with increasing amounts of unlabeled β-CIT (at 2-fold the final desired concentrations). The assay was started by adding 30 μL of diluted membranes to each well. Binding was allowed to proceed for 1−1.5 h at room temperature with gentle rocking. The reaction was stopped by washing all wells 3× with 200 μL of ice-cold binding buffer. The filters were punched out of the plate and counted after overnight soaking in 3 mL of Optifluor. The binding affinity (K_D) and maximal binding capacity (B_{max}) for β-CIT were determined by fitting the binding curves using the Origin plotting program (MicroCal Software, Northampton, MA). Values reported in Table 3 represent the mean and standard deviation of two to four separate assays. Graphs show representative curves.

Serotonin affinity was also measured by the displacement of [^{125}I]-β-CIT from the membranes. Under the conditions used, where the concentration of β-CIT is below its K_D, the concentration at which half the β-CIT is displaced by serotonin (K_I) represents the K_D for serotonin. Assays were performed exactly as for the β-CIT curves, except that increasing amounts of serotonin were added to each well together with a constant, low concentration of β-CIT. The K_i was determined by fitting the resulting inhibition curves using the Origin program. Again, values reported in Table 3 represent the mean and standard deviation of two to four separate assays, and graphs show representative curves.

Determination of Cell Surface Expression. Cell surface expression of mutant and wild-type SERTs was determined using the membrane-impermeant biotinylating reagent NHS-SS-biotin (sulfosuccinimidyl-2-(biotinamido) ethyl-1,3-dithiopropionate; Pierce Chemical Co., Rockford, IL). HeLa cells were grown and transfected as described above for transport except in 12 well plates, again with appropriate scaling up of DNA and other reagents. Eighteen to 24 h post-transfection, each well was washed twice with 1.2 mL of room-temperature PBSCM. After removing the second wash, 500 μL of 1.5 mg/mL NHS-SS-biotin freshly dissolved in biotinylation buffer (20 mM Na-HEPES (pH 8.5), 2 mM $CaCl_2$, 150 mM NaCl) was added to each well. Cells were allowed to incubate for 20 min at room temperature, the reagent was removed, and the cells were incubated in a second freshly prepared NHS-SS-biotin solution. The reaction was stopped by removing the biotinylating reagent and washing the cells twice with ice-cold PBSCM containing 100 mM glycine, which reacts with any leftover reagent. The NHS-SS-biotin-labeled cells were lysed in 100 μL of SDS-lysis buffer (50 mM Tris (pH 7.5), 150 mM NaCl, 5 mM EDTA, 1% Triton X-100, 1% SDS, 0.2 mM PMSF, and 0.5% Sigma Protease Inhibitor Cocktail) for 30 min on ice. The cell lysate was diluted to 1.2 mL with ice-cold Lysis buffer (same as SDS-lysis buffer above but without SDS or protease inhibitors). The biotinylated proteins were recovered by overnight incubation with 100 μL of streptavidin-agarose beads per sample (Pierce Chemical Co., Rockford, IL) at 4 °C with end-over-end rotation. The next day, the beads were washed once with 1.2 mL of Lysis buffer, once with 1.2 mL of High Salt lysis buffer (same as Lysis buffer except with 500 mM NaCl and 0.1% Triton X-100), and twice with 1.2 mL of 50 mM Tris, pH 7.5. The biotinylated proteins were eluted using 100 μL of SDS−PAGE sample buffer (62.5 mM Tris (pH 6.8), 2% SDS, 10% glycerol, 1% mercaptoethanol, 0.003% bromphenol blue) for 10 min at 85 °C. One-fifth of each sample was applied to a 10% SDS−PAGE gel (Laemmli protocol (*34*)) and transferred to nitrocellulose for Western blotting (Towbin protocol (*35*)).

Wild-type SERT and mutant transporters were detected in the mixture of biotinylated proteins using the M2 anti-FLAG antibody (Sigma Chemical Co.) directed against the FLAG epitope tag located at the C-terminus. Blots were incubated with 10 μg/mL anti-FLAG in blocking buffer (5% nonfat dry milk, 40 mM Tris (pH 7.5), 300 mM NaCl, 0.1% Tween 20) overnight with gentle rocking, washed, and then further incubated with goat anti-mouse IgG-horseradish

peroxidase conjugate (Pierce). After further washing, bands were detected by chemiluminesence using Super Signal West Pico detection reagent (Pierce). Total cell expression levels were determined without biotinylation by lysing cells directly in SDS−PAGE sample buffer, heating to 85 °C for 10 min, and applying them to an SDS−PAGE gel without further sample preparation.

RESULTS

Site-directed mutagenesis studies had shown that substitution of Val-382 with proline in rat SERT yields a completely nonfunctional transporter (*10*). Given the known properties of the TP motif (*20*), we hypothesized that the kink induced by the V382P mutation was exacerbated by the presence of a threonine residue at the adjacent 381 position (Figure 1). We tested this hypothesis by exploring the conformational space accessible to TM7 in the WT and three mutant constructs: V382P (TP), T381A-V382P (AP), and T381V-V382P (VP). The activities of these mutants were then characterized biochemically by the measurement of serotonin uptake, substrate and inhibitor binding, and cell surface expression levels.

Computational Analysis of TM7 Mutant Structures. Comparative analysis of the structure and orientation of the helix in WT and the TP, AP, and VP mutants shows that the structures of the three mutants cluster in different regions of three-dimensional space, with some overlap among them. However, there is no overlap between these clusters and the single main cluster obtained for WT. To quantify the comparison of the ensemble of structures calculated for the WT and mutant helices, we defined the geometry of the kink as described earlier (*19*) in terms of the bend and wobble angles. The bend angle describes the magnitude of the angle formed between the helix segments preceding and following the proline residue. In an ideal helix, the average bend angle would be near zero (i.e., <10°). The wobble angle describes the orientation of this bend with respect to the α carbon of the proline residue. This angle describes the position in three-dimensional space of the segment following the proline with respect to the axis established by the helix segment preceding the proline (see Figure 2).

Bend Angles. The ensembles of structures obtained for the TP, AP, and VP mutants cover different areas of the conformational space but with considerable overlap. For the WT helix, the average value of the bend angle $\langle\theta\rangle$, as defined in Experimental Procedures, is 10.3°, which falls in the first bin, including bend angles between 0 and 15° (Table 1). The population of this bin is defined by $P(\theta)$ (see Experimental Procedures) and has a value of 91%, indicating that 91% of all the structures fall in the narrow region between 0 and 15°. Interestingly, the population of the same area in the mutant helices is at or near 0% (Table 1). These results indicate that the WT helix is straight but may prefer a small kink because of the presence of threonine, which has been reported recently to induce a small bend in α-helices (*36*). In contrast, the average value of the bend angle in the TP mutant helix is $\langle\theta\rangle_b = 31.6°$, and the most populated region is between 30 and 35°, containing 41.5% of the structures (Table 1). The population of the same region in the AP mutant drops to 21.6% (Table 1). The most populated region for the AP mutant lies between 25 and 30° (50% of the structures; Table 1). For the VP mutant, the region between angles 20 and 25° is the most populated one with a probability of 46% (Table 1).

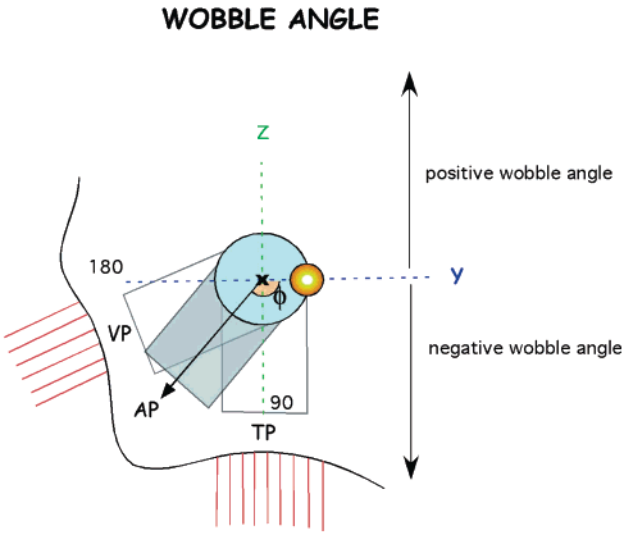

FIGURE 2: Cartoon representation of the three-dimensional space swept by the wobble angle. The helix fragments preceding and following the proline are represented as simple cylinders. The viewer looks at the helix from the bottom of the helix fragment preceding the proline; thus, this helix cylinder would be seen as a circle and is represented in the figure as a blue circle. The fragment of helix following the proline is kinked and in this simplification would be viewed as a cylinder at an angle and thus is represented in two dimensions in the figure as a blue rectangle. Because it is viewed end on, the magnitude of the kink itself (the bend angle) is not apparent to the viewer. The *x* in the center represents the axes of the helix preceding the proline, which is used as screw axis to define the wobble angle (see refs *18* and *19*). The proline C-α carbon is represented by an orange sphere. The wobble angle ϕ defines the orientation of the kink with respect to C-α (for a more detailed description see refs *18* and *19*)). The ensemble of structures obtained for the V382P (TP) and T381V-V382P (VP) mutants clustered around −90° and close to −180°, respectively. The detrimental effect of both mutations is likely because of tight packing of the bundle in those regions as indicated in the cartoon by the red dashed areas. The T381A-V382P (AP) mutant bends toward wobble angle values comprised between −100 and −140°. The higher tolerance for this mutation indicates a more permissive packing in that area. The wild-type helix itself does not contain a proline and possesses only a very small calculated kink. For the purposes of this analysis the wild-type helix was considered to be an ideal helix. It can be visualized as a straight cylinder perpendicular to the plane of the page, passing through the blue circle, with no kink or wobble.

Table 1: Population of Bend Angle Bins for TM7 Conformations in the V382P (TP), T381A-V382P (AP), and T381V-V382P (VP) Mutants and WT SERT Obtained from Independent Monte Carlo Simulations[a]

	0−15	15−20	20−25	25−30	30−35	35−40	>40
TP	0	0	4.3	28.6	41.5	21.5	2.7
AP	0	0	21.7	50	21.6	5	1.7
VP	3.5	0	46	34	5	5	6.5
WT	91	0	0	0	0	0	9

[a] The population reflects an energy weighted probability of finding an structure with a bend angle in each particular interval ($P(\theta)$, eq 2).

Wobble Angles. Table 2 shows the most populated regions for the wobble angle in the mutant structures (no wobble angle is reported for the wild-type structure since it contains no proline kink). The average wobble angle for the TP mutant is $\langle\theta\rangle_w = -95.5°$, with 41.5% of the structures found in the

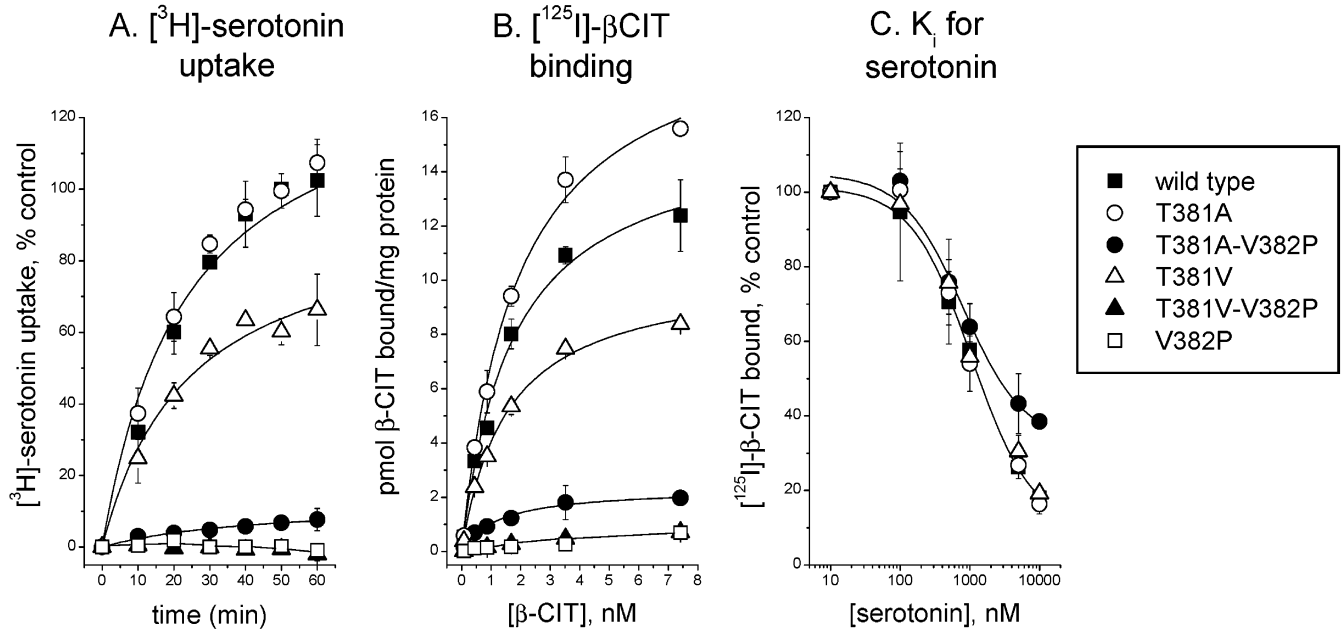

FIGURE 3: Functional characteristics of the VP (T381V-V382P) and AP (T381A-V382P) mutants as compared to the control mutants, T381A and T381V, and wild-type SERT. Serotonin transporter mutants were transiently expressed in HeLa cells and [^{3}H]-serotonin uptake, [^{125}I]-β-CIT binding, and serotonin displacement of β-CIT binding were measured as described in Experimental Procedures. (A) [^{3}H]-Serotonin uptake with time. (B) Saturation curves for [^{125}I]-β-CIT binding. (C) Competitive inhibition of β-CIT binding by increasing concentrations of serotonin. Panel A represents a composite of several experiments, while panels B and C are the results of single experiments. Error bars smaller than the width of the symbols have been omitted.

Table 2: Population of Wobble Angle Bins for TM7 Conformations in the V382P (TP), T381A-V382P (AP), and T381V-V382P (VP) Mutants Obtained from Independent Monte Carlo Simulations[a]

	>−80	−80 to −100	−100 to −120	−120 to −140	−140 to −160	−160 to −180
TP	6.9	41.5	40.1	11.4	0	0
AP	1.7	11.6	40	40	3.3	3.3
VP	31.8	0	0	8.5	30.7	28.9

[a] The population reflects an energy weighted probability of finding a structure with a bend angle in each particular interval ($P(\theta)$, eq 2).

Table 3: Binding Parameters of Mutants T381A-V382P, T381A, and T381V as Compared to Those of WT SERT[a]

mutant	K_D for β-CIT (nM)	B_{max} for β-CIT (pmol/mg protein)	K_I for serotonin (nM)
WT	1.9 ± 1.2	12.0 ± 5.2	996 ± 241
T381A-V382P (AP)	1.2 ± 0.4	1.7 ± 0.9[b]	596 ± 194
T381A	2.4 ± 0.6	16.2 ± 5.4	1224 ± 316
T381V	2.3 ± 1.1	8.5 ± 2.8	1150 ± 95

[a] Binding of β-CIT and displacement by serotonin were measured as described in Experimental Procedures. [b] Statistically significant difference from wild type by *t*-test, $p < 0.05$).

region between −80 and −100° (Table 2). The same region for the AP mutant has a population of only 11.6% of the total (Table 2). The wobble angle of the TP and AP mutants overlaps in the region corresponding to bin −100 to −120°, spreading toward higher values of the wobble angle in the case of the AP mutant and lower values of wobble angle for the TP mutant. The VP mutant clusters mainly in the region between angles of −140 and −180°. These results for the wobble angle are illustrated graphically in Figure 2.

Taken together, the results of the structural analysis show that the V382P mutant, containing the TP motif, tends toward higher bend angles and a different region of the conformational space than the double mutants T381A-V382P and T381V-V382P, in which the TP motif is eliminated, but the proline is preserved.

Experimental Analysis of TM7 Mutant Activities. Serotonin Uptake. Figure 3A shows the time course of transport activity for wild-type SERT, the double mutants AP and VP, and the single mutants T381A, T381V, and V382P. The VP double mutant showed no detectable transport activity, even after 1 h of incubation with [^{3}H]-serotonin, similar to the V382P parent. However, the substitution of alanine at position 381 allowed partial recovery of transport activity in the AP mutant, albeit to a low level (8 ± 3% of wild type at its maximum). As controls, the individual mutations T381A and T381V were also tested for their effects on SERT transport activity. Mutation T381A had no apparent effect on transport activity. Mutation T381V reduced transport activity to 60 ± 4% of the wild-type level at its maximum.

Binding of β-CIT and Serotonin. To further characterize the nature of the defect in mutant V382P that is partially rescued by the T381A mutation, we investigated the affinity of the mutant transporters for the competitive inhibitor β-CIT and the substrate serotonin. Figure 3B shows [^{125}I]-β-CIT saturation binding curves for the wild type and mutants. Again, the addition of the T381A mutation to the V382P mutant construct restored a low level of activity in the AP mutant. As for transport, mutation T381V was unable to restore activity in the VP double mutant. Table 3 shows the binding parameters derived from these data for the mutants with detectable binding. Although mutants T381A and T381V showed slightly higher and lower mean B_{max} values, respectively, than wild type, these differences were not statistically significant. The AP mutant showed a mean B_{max} of 1.7 ± 0.9 pmol/mg protein, which was a statistically significant difference (16% of WT binding, see Table 3).

Since these experiments were done in membrane preparations, this value represents the amount of AP mutant protein that was correctly folded both on the cell surface and in intracellular pools. This fraction is higher than the amount of correctly folded AP mutant that reached the cell surface, as indicated by transport activity, which was 8% of the wild type. Both fractions are substantially larger than for the VP mutant, which did not show any detectable transport or binding (Figure 3A,B). All of the mutants with detectable binding showed an affinity for β-CIT (K_D) very similar to wild type (Table 3).

The serotonin affinity of each mutant was determined by measuring the ability of unlabeled serotonin to competitively displace [^{125}I]-β-CIT binding. Figure 3C shows competition curves for each mutant with detectable binding (T381A-V382P, T381A, and T381V) and for wild type. Increasing concentrations of serotonin were added to membrane preparations at a constant concentration of β-CIT, lying below its K_D. Under these conditions, the $K_{1/2}$ for serotonin displacement of β-CIT closely approximates the binding affinity (K_D) for serotonin. Figure 3C shows that the competition curves were virtually superimposable, indicating that all of the mutants had the same serotonin affinity as the wild type. The serotonin affinities derived from several repetitions of these experiments are shown in Table 3.

Cell Surface Expression. Since transport into whole cells requires transporter on the cell surface, transport activity is a partial measurement of cell surface expression. As a more direct measurement, we determined cell surface expression using the membrane-impermeant biotinylating reagent NHS-SS-biotin. This reagent reacts with lysine residues on the extracellular surface of membrane-bound proteins, including SERT. This method has been used previously to measure the cell surface expression of mutant SERTs (*5*, *33*, *37*). Unlike uptake measurements, this method can detect transporter molecules that may reach the cell surface but are nonfunctional because of improper folding. Figure 4 shows the results of this analysis. As shown in the upper panel (lane 2), wild type (tagged) SERT presents a complex pattern on Western blots of whole cell extracts (total expression). Three major bands appear, at approximately 200, 150, and 50−60 kDa (marked with arrows). An additional diffuse band appears at 90 kDa (marked with an asterisk). This 90 kDa band is thought to represent the mature glycosylated transporter because it is highly enriched in the biotinylated, cell surface fraction (compare to lane 2, bottom panel). This conclusion is further supported by the observation that native SERT isolated from both rat brain and rat platelets also runs as a single, diffuse band of 80−90 kDa (*38*). In these tissues, and in the HeLa cell system as well, the 90 kDa band is reduced to 60 kDa by treatment with PNGase F (*38*) indicating that it is glycosylated. Thus, the 50−60 kDa band most likely represents immature, unglycosylated transporter. The upper bands (200 and 150 kDa) are probably aggregates of the lower molecular weight forms, a common occurrence with highly hydrophobic membrane proteins on SDS−PAGE gels.

Figure 4 shows that, of the mutant transporters, only the single mutants T381A and T381V contain a detectable amount of the 90 kDa band in the cell surface fraction (lanes 4 and 6, lower panel). This result correlates well with their nearly wild-type levels of transport and binding (Figure 3).

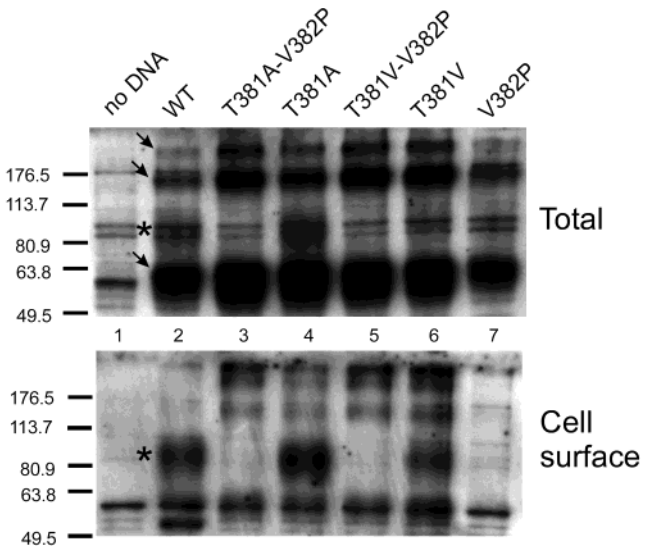

FIGURE 4: Cell surface expression of wild type and mutant serotonin transporters. Wild type and mutant SERTs were expressed in HeLa cells, and total (upper panel) and cell surface (lower panel) expression were measured using cell surface biotinylation and Western blotting as described in Experimental Procedures. Arrows mark the three major bands seen in total cell extracts of cells expressing wild-type SERT (200, 150, and 60 kDa). Asterisks mark the major cell surface form of the protein that is enriched in the cell surface (biotinylated) fraction (90 kDa). Total expression samples represent 5% of the material from one well of a 24-well plate, while cell surface samples represent 60% of the material from one well (12-fold concentrated compared to total expression.)

In particular, the 90 kDa band appears to be slightly reduced in the T381V mutant, which may correlate with its slightly lower transport activity (60% of WT). V382P and the double mutants, on the other hand, which have no or very low transport and binding activities, do not show detectable amounts of the 90 kDa form. Nearly all of the lanes also show some amount of the 200, 150, and 50−60 kDa bands in the cell surface fraction. The relative amounts of these forms do not correlate with the levels of transport activity in each mutant. Their presence is most likely because of penetration of the biotinylating reagent into a small fraction of dead or dying cells. This fraction would be similar for all of the mutants since they were all transfected under the same conditions. It can be seen from the total expression lanes (Figure 4, upper panel) that these forms are much more abundant than the mature 90 kDa form. This overabundance is due to the high level of overexpression in this system, which presumably overwhelms the cells' processing machinery and results in a large amount of immature SERT that does not reach the cell surface. Because of the relative overabundance of this immature SERT, penetration of a small number of dead cells by the biotinylating reagent leads to the presence of these bands in the biotinylated fraction. It is important to note that the material loaded in the biotinylated wells (lower panel) represents 12-fold more than was loaded in the total expression wells (upper panel). We quantitated the fraction of the 50−60 kDa band in WT that is carried over into the biotinylated fraction by area densitometry of the digital image. Taking into account the 12-fold higher loading in the lower panel, this fraction was 3.4%. This is close to the 5% fraction of dead cells that we have previously measured by trypan blue exclusion for HeLa cell cultures under these transfection conditions (M. Stephan, unpublished

results). Thus, we are confident that, by focusing on the 90 kDa band, we are accurately comparing the cell surface levels of the WT and mutant SERTs.

DISCUSSION

In a previous study, we used random site-directed mutagenesis to investigate the role of transmembrane span 7 in SERT structure and function (*10*). We identified a number of functionally important residues in TM7 that were highly sensitive to mutation. The pattern of these residues suggested that they lie along one side of an α-helix. In addition, analysis of conserved residues between SERT and the other members of the NaCl dependent transporter superfamily indicated the presence of a highly hydrophobic region from residues 361−387, with the characteristics of an amphipathic helix (Figure 1) (*13*). The conservation pattern of the first half of this region, comprising residues Ala-361 to Ser-375, shows a helical periodicity in which the conserved face corresponds to the polar one (*13*) and coincides as well with the functionally critical residues identified by mutagenesis (*10*). This pattern indicates that this more intracellular half of TM7 is likely to be exposed to the membrane along one side. By contrast, the other, more extracellular half (residues Gly-376 to Ala-387) consists of 12 sequential highly conserved residues, indicating that this part of the helix is likely to lie buried in the protein core, where it may form important contacts with other helices (*13*). In this paper, we present both computational and biochemical studies supporting the hypothesis that the conformation of this extracellular half of TM7 plays an integral role in maintaining SERT's ability to achieve a mature, cell surface conformation.

Among the mutations obtained in the previous study were four proline substitutions, at positions 361, 371, 381, and 382. Two of these mutants, T371P and V382P, were completely nonfunctional, as might be expected if the known perturbation caused by proline in α-helices was detrimental to function. Interestingly, however, proline substitutions were somewhat tolerated in mutants A361P and T381P (transport activities were 46 ± 14 and 45 ± 5% of wild type, respectively (*10*)). In the case of A361P, the ability to tolerate a proline might be explained by the fact that this residue lies very near the end of the predicted membrane-spanning helix, possibly even lying outside the α-helical region. In the case of T381P, however, it was particularly puzzling that a proline was somewhat tolerated here but not at the adjacent position in mutant V382P.

These considerations suggested that the perturbation introduced by the V382P mutation might somehow disrupt the packing of the helices surrounding the top of TM7, and further, that the strong phenotype of the V382P mutation might be due to the presence in the native sequence of a threonine at position 381. As described previously, the TP motif created by the presence of a threonine at $i - 1$ from the proline is characterized by a larger kink than the one produced when proline is preceded by non-hydrogen bonding residues, and its presence can have significant functional consequences (*18*, *20*, *22*). To test this hypothesis, we have investigated the effect of the residue preceding V382P on the structure of SERT TM7 by using biased Monte Carlo simulations to explore the conformational preferences of the WT as compared to the V382P mutant.

We find that the substitution of residue V382 by proline produces a change in the distribution of energetically accessible structures in models of TM7. All of the mutant constructs we evaluated (V382P, T381A-V382P, and T381V-V382P) were predicted to have larger bend angles than the WT. In particular, the bend angle for the V382P construct (with a TP-motif in its sequence) showed the highest values (Table 1). These larger bend angles, on the order of 20−40°, could produce considerable structural disruption. It can be calculated from simple geometrical considerations that, if a proline is positioned in the middle of a TM helix, about 18 Å from an end, then >3 Å are added to the distance from the center for every 10° in bending. This change in distance could have significant functional consequences. For example, a 6−10 Å departure in TM6 of rhodopsin is enough to produce the activated form that interacts with the G protein (*39*).

Interestingly, the bend angle in the T381V-V382P mutant is predicted by the computational studies to be smaller than in the T381A-V382P mutant. Thus, it might have been expected that the reduction of the kink angle in the case of the T381V-V382P as compared to V382P would lead to a better recovery of activity. However, modeling of this mutant indicated the presence of a different structural perturbation, characterized by a different wobble angle value (Table 2), which is likely to explain the lack of recovery in this mutant. Figure 2 graphically illustrates the wobble angle, which represents the three-dimensional orientation of the kink with respect to the position of the proline C-α. The residue at position $i - 1$ from the proline would lie at an angle θ of approximately −110°. In the model of the V382P mutant, a threonine residue at that position makes a hydrogen bond with the carbonyl oxygen at position $i - 4$ (*20*). This hydrogen bond forces the kink of the helix in the same direction, resulting in a larger kink angle and a wobble angle that oscillates around −110°. Such dramatic structural effects of TP motifs are observed in the TMs of membrane proteins with known structure. For example, in cytochrome C oxidase (1EHK), the 262−285 helix has a TP motif (277−278) with a calculated bend angle of 41.8° and a wobble angle of 131.9°; similarly, the ACRB multidrug efflux transporter (1IWG) has a TP motif (489−490) in the TM helix (463−496) with a bend angle of 30.4° and a wobble angle of −32.2°.

In contrast, in the model of the T381V-V382P mutant, the valine residue at $i - 1$ positions its γ-methyl group toward the preceding turn thereby impairing the bending of the helix toward itself. This explains why the wobble angle for the double T381V-V382P mutant avoids the region between values −100 to −140° and tends to values closer to −180°.

The biochemical data presented here show that, as predicted by structural analysis, the addition of the T381A mutation to the V382P mutant resulted in restoration of SERT expression, albeit only partially. Mutant V382P is highly impaired in serotonin transport, β-CIT binding activity, and in its ability to reach the cell surface (Figures 3 and 4). The addition of the T381A mutation resulted in partial recovery of all three of these activities (Figure 3 and Table 3). Although cell surface expression of this mutant was still too low to be detected directly by cell surface biotinylation (Figure 4), partial restoration of cell surface expression is

demonstrated by the ability of the T381A-V382P mutant to transport serotonin, which cannot occur unless at least some transporter is reaching the cell surface.

The results of Western blotting from whole cell extracts (Figure 4) show that the V382P mutant protein accumulates in the cell at levels similar to wild type. Thus, the defect in this mutant does not lie in the early stages of protein synthesis but must lie in one or more of the later steps of protein folding, maturation, and delivery to the cell surface. The lack of β-CIT binding activity in membrane preparations shows that, in addition to failing to reach the cell surface, internal pools of the V382P mutant protein are not properly folded. It is not possible from these data to determine more exactly what stage of SERT biosynthesis or folding, or both, is affected by the distortion created in the V382P mutant or the extent to which this misfolding is rescued by the addition of the T381A mutation. However, the fact that the V382P mutation affects two disparate aspects of SERT function, the ability of SERT to form a β-CIT binding site and its ability to be recognized by the processes responsible for delivery to the cell surface, suggests that the structure of the V382P mutant is likely to be significantly divergent from wild type. This result demonstrates the critical role of TM7 structure in the ability of SERT to achieve a properly folded, cell surface configuration.

Notably, the T381V mutation alone had a detrimental effect on SERT function, reducing transport activity by 40% (Figure 3). If the T381V mutation did relieve the disruptive effects of the predicted TP-induced kink, the rescued activity would most likely be very low (as for the T381A-V382P construct), and a further 40% reduction would make it difficult to distinguish this activity from background. The detrimental effect of the single substitution of T381V may be due to the introduction of a bulkier residue as compared with threonine. If this region of the bundle is tightly packed, as we infer, then the additional volume would be likely to interfere with the surrounding residues.

The hypothesis that TM7 plays an integral role in the ability of SERT to mature into a fully active, cell surface conformation is supported by the results of previous studies, both from our group using SERT (*10*), and from others studying its close relatives the dopamine and norepinephrine transporters (DAT and NET, respectively). Early studies of chimeras between DAT and NET showed that chimeras with junction points lying within or between TMs 5 and 8 were completely nonfunctional, suggesting that these TMs might form the structural core of the protein (*40*). Later studies have shown that point mutations in DAT TM7 have broad, diverse effects on transporter structure, function, and cell surface expression (*14*−*16*, *41*). We have also identified multiple functional defects in SERT TM7 mutants, including indirect effects on ion binding and the coupling of Na^+ to serotonin transport (*10*, *42*).

In addition to its role as an important structural element in SERT, there is evidence that TM7 participates in the conformational changes associated with the translocation of serotonin across the membrane. Mutants in the serine residues in NET showed altered rates of efflux, suggesting that these mutations were involved in or somehow influenced the transport mechanism (*43*). TM7 is further implicated in transport by studies of endogenous and engineered zinc binding sites in DAT suggesting that zinc inhibits dopamine transport by preventing the movement of TM7 and/or the fourth extracellular loop relative to other parts of the protein (*13*). Consonant with these inferences are results from studies showing that mutations in TM7 can alter conformational changes in the first external loop (*42*). These previous studies indicate that TM7 plays an important role in SERT function. The results presented here show that TM7 also plays an important role in the structural integrity and biosynthesis of SERT since structural perturbations in TM7 lead to both improper folding and loss of cell surface expression, and modulation of these perturbations can restore these properties. Taken together, these results support our hypothesis that TM7 is a key structural and functional element of SERT that is most likely buried among other helices in the core of the transporter's three-dimensional structure.

ACKNOWLEDGMENT

We thank Thijs Beuming for help with the bioinformatics analysis.

REFERENCES

1. Saier, M. H., Jr. (1999) *J. Cell. Biochem. 75*, 84−94.
2. Blakely, R. D., DeFelice, L. J., and Hartzell, H. C. (1994) *J. Exp. Biol. 196*, 263−81.
3. Kanner, B. I. (1994) *J. Exp. Biol. 196*, 237−49.
4. Rudnick, G. (1998) *J. Bioenerg. Biomembr. 30*, 173−85.
5. Chen, J. G., Liu-Chen, S., and Rudnick, G. (1998) *J. Biol. Chem. 273*, 12675−81.
6. Androutsellis-Theotokis, A., Ghassemi, F., and Rudnick, G. (2001) *J. Biol. Chem. 276*, 45933−8.
7. Androutsellis-Theotokis, A., and Rudnick, G. (2002) *J. Neurosci. 22*, 8370−8.
8. Reith, M. E. A. (1997) in *Neurotransmitter Transporters. Structure, Function and Regulation.* (Reith, M. E. A., Ed.) pp 1−28, Humana Pres Inc., Totowa, NJ.
9. Visiers, I., Ballesteros, J. A., and Weinstein, H. (2002) *Methods Enzymol. 343*, 329−71.
10. Penado, K. M., Rudnick, G., and Stephan, M. M. (1998) *J. Biol. Chem. 273*, 28098−106.
11. Norregaard, L., Frederiksen, D., Nielsen, E. O., and Gether, U. (1998) *EMBO J. 17*, 4266−73.
12. Loland, C. J., Norregaard, L., and Gether, U. (1999) *J. Biol. Chem. 274*, 36928−34.
13. Norregaard, L., Visiers, I., Loland, C. J., Ballesteros, J., Weinstein, H., and Gether, U. (2000) *Biochemistry 39*, 15836−46.
14. Kitayama, S., Shimada, S., Xu, H. X., Markham, L., Donovan, D. M., and Uhl, G. R. (1992) *Proc. Natl. Acad. Sci. U.S.A. 89*, 7782−5.
15. Kitayama, S., Wang, J. B., and Uhl, G. R. (1993) *Synapse 15*, 58−62.
16. Lin, Z., Wang, W., Kopajtic, T., Revay, R. S., and Uhl, G. R. (1999) *Mol. Pharmacol. 56*, 434−47.
17. Loland, C. J., Norregaard, L., Litman, T., and Gether, U. (2002) *Proc. Natl. Acad. Sci. U.S.A. 99*, 1683−8.
18. Sansom, M. S., and Weinstein, H. (2000) *Trends Pharmacol. Sci. 21*, 445−51.
19. Visiers, I., Braunheim, B., and Weinstein, H. (2000) *Protein Eng. 13*, 603−6.
20. Ri, Y., Ballesteros, J. A., Abrams, C. K., Oh, S., Verselis, V. K., Weinstein, H., and Bargiello, T. A. (1999) *Biophys. J. 76*, 2887−98.
21. Cordes, F. S., Bright, J. N., and Sansom, M. S. P. (2002) *J. Mol. Biol. 323*, 951−60.
22. Jin, T., Peng, L., Mirshahi, T., Rohacs, T., Chan, K. W., Sanchez, R., and Logothetis, D. E. (2002) *Mol. Cell Biol. 10*, 469−81.
23. Brooks, B. R., Bruccoleri, R. E., Olafson, B. D., States, D. J., Swaminathan, S., and Karplus, M. (1983) *J. Comput. Chem. 4*, 187−217.
24. Sankararamakrishnan, R., and Vishveshwara, S. (1992) *Int. J. Pept. Protein Res. 39*, 356−63.
25. Guarnieri, F., and Wilson, S. R. (1995) *J. Comput. Chem. 16*, 648−53.

26. Guarnieri, F., and Weinstein, H. (1996) *J. Am. Chem. Soc. 118*, 5580−9.
27. Sarkar, G., and Sommer, S. S. (1990) *BioTechniques 8*, 404−7.
28. Barik, S., and Galinski, M. S. (1991) *BioTechniques 10*, 489−90.
29. Aiyar, A., and Leis, J. (1993) *BioTechniques 14*, 366−9.
30. Tate, C. G., and Blakely, R. D. (1994) *J. Biol. Chem. 269*, 26303−10.
31. Elroy-Stein, O., Fuerst, T. R., and Moss, B. (1989) *Proc. Natl. Acad. Sci. U.S.A. 86*, 6126−30.
32. Blakely, R. D., Clark, J. A., Rudnick, G., and Amara, S. G. (1991) *Anal. Biochem. 194*, 302−8.
33. Stephan, M. M., Chen, M. A., Penado, K. M., and Rudnick, G. (1997) *Biochemistry 36*, 1322−8.
34. Laemmli, U. K. (1970) *Nature 227*, 680−5.
35. Towbin, H., Staehelin, T., and Gordon, J. (1979) *Proc. Natl. Acad. Sci. U.S.A. 76*, 4350−4.
36. Ballesteros, J. A., Deupi, X., Olivella, M., Haaksma, E. E., and Pardo, L. (2000) *Biophys. J. 79*, 2754−60.
37. Smicun, Y., Campbell, S. D., Chen, M. A., Gu, H., and Rudnick, G. (1999) *J. Biol. Chem. 274*, 36058−64.
38. Qian, Y., Melikian, H. E., Rye, D. B., Levey, A. I., and Blakely, R. D. (1995) *J. Neurosci. 15*, 1261−74.
39. Farrens, D. L., Altenbach, C., Yang, K., Hubbell, W. L., and Khorana, H. G. (1996) *Science 274*, 768−70.
40. Buck, K. J., and Amara, S. G. (1994) *Proc. Natl. Acad. Sci. U.S.A. 91*, 12584−12588.
41. Itokawa, M., Lin, Z., Cai, N. S., Wu, C., Kitayama, S., Wang, J. B., and Uhl, G. R. (2000) *Mol. Pharmacol. 57*, 1093−103.
42. Kamdar, G., Penado, K. M., Rudnick, G., and Stephan, M. M. (2001) *J. Biol. Chem. 276*, 4038−45.
43. Danek Burgess, K. S., and Justice, J. B., Jr. (1999) *J. Neurochem. 73*, 656−664.

BI0273415